

Alteration of the Flexible Loop in 1-Deoxy-D-xylulose-5-phosphate Reductoisomerase Boosts Enthalpy-Driven Inhibition by Fosmidomycin

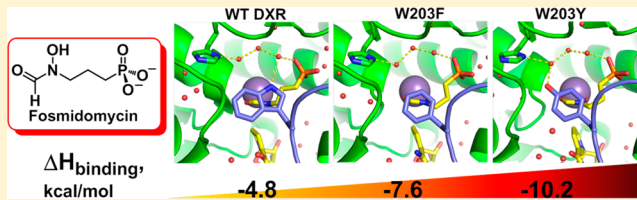
Svetlana A. Kholodar,[†] Gregory Tomblin,[†] Juan Liu,[†] Zhesen Tan,[†] C. Leigh Allen,[‡] Andrew M. Gulick,[‡] and Andrew S. Murkin^{*,†}

[†]Department of Chemistry, University at Buffalo, Buffalo, New York 14260-3000, United States

[‡]Hauptman-Woodward Institute and Department of Structural Biology, University at Buffalo, Buffalo, New York 14203-1102, United States

Supporting Information

ABSTRACT: 1-Deoxy-D-xylulose-5-phosphate reductoisomerase (DXR), which catalyzes the first committed step in the 2-C-methyl-D-erythritol 4-phosphate pathway of isoprenoid biosynthesis used by *Mycobacterium tuberculosis* and other infectious microorganisms, is absent in humans and therefore an attractive drug target. Fosmidomycin is a nanomolar inhibitor of DXR, but despite great efforts, few analogues with comparable potency have been developed. DXR contains a strictly conserved residue, Trp203, within a flexible loop that closes over and interacts with the bound inhibitor. We report that while mutation to Ala or Gly abolishes activity, mutation to Phe and Tyr only modestly impacts k_{cat} and K_m . Moreover, pre-steady-state kinetics and primary deuterium kinetic isotope effects indicate that while turnover is largely limited by product release for the wild-type enzyme, chemistry is significantly more rate-limiting for W203F and W203Y. Surprisingly, these mutants are more sensitive to inhibition by fosmidomycin, resulting in K_m/K_i ratios up to 19-fold higher than that of wild-type DXR. In agreement, isothermal titration calorimetry revealed that fosmidomycin binds up to 11-fold more tightly to these mutants. Most strikingly, mutation strongly tips the entropy–enthalpy balance of total binding energy from 50% to 75% and 91% enthalpy in W203F and W203Y, respectively. X-ray crystal structures suggest that these enthalpy differences may be linked to differences in hydrogen bond interactions involving a water network connecting fosmidomycin’s phosphonate group to the protein. These results confirm the importance of the flexible loop, in particular Trp203, in ligand binding and suggest that improved inhibitor affinity may be obtained against the wild-type protein by introducing interactions with this loop and/or the surrounding structured water network.



I soprenoids are essential secondary metabolites that are assembled from the five-carbon units isopentenyl pyrophosphate and dimethylallyl pyrophosphate. These building blocks are the products of one of two biosynthetic pathways that are differentially distributed throughout various organisms: whereas humans and other animals utilize the mevalonate pathway, certain species of bacteria, protozoa, and plants have evolved an independent pathway known as the non-mevalonate or 2-C-methyl-D-erythritol 4-phosphate (MEP) pathway.¹ Importantly, none of the seven enzymes comprising the MEP pathway have homologues in humans,² making them attractive targets for the development of selective drugs against many human pathogens, including *Mycobacterium tuberculosis* and *Plasmodium falciparum*.³

The first committed step in the MEP pathway is governed by 1-deoxy-D-xylulose-5-phosphate (DXP) reductoisomerase (DXR), which catalyzes a retroaldol–aldol rearrangement of DXP,^{4,5} followed by reduction by NADPH to yield MEP (Scheme 1). Fosmidomycin is a natural product produced by *Streptomyces* bacteria that inhibits DXR with K_i values in the

range of 10^{-8} to 10^{-7} M.^{6–9} Although it is effective in the treatment of malaria caused by *P. falciparum*,^{10,11} fosmidomycin, its acetyl analogue, and their phosphonate ester prodrugs are poorly active against *M. tuberculosis*.^{12,13} Understanding the nature of interactions between fosmidomycin and DXR for the purposes of designing improved alternatives is therefore invaluable.

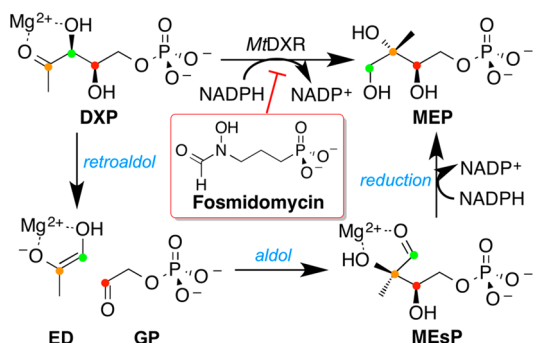
Alignment of DXR sequences from several pathogens revealed a highly conserved HPXWXMG motif that forms a flexible loop that exists in a closed conformation when fosmidomycin or another dianion (i.e., DXP, sulfate,¹⁴ or phosphite¹⁵) is bound and in an open conformation when this ligand is absent (Figure 1).¹⁶ Of particular note in this flexible loop is Trp203 (numbering based on DXR from *M. tuberculosis*, MtDXR), whose indole ring is believed to protect the active site from bulk solvent.¹⁶ However, a direct link between this residue

Received: April 4, 2014

Revised: April 30, 2014

Published: May 13, 2014

Scheme 1. Mechanism of MtDXR-Catalyzed Conversion of DXP to MEP^a



^aAbbreviations: DXP, 1-deoxy-D-xylulose 5-phosphate; MEP, 2-C-methyl-D-erythritol 4-phosphate; ED, enediolate [(Z)-propene-1,2-diolate]; GP, glycolaldehyde 2-phosphate; MEsP, 2-C-methyl-D-erythrose 4-phosphate.

(or the loop as a whole) and catalytic events has yet to be established. In this work, we have addressed this concern using site-directed mutagenesis together with steady-state kinetics, pre-steady-state kinetics, and kinetic isotope effects. Moreover, we evaluated inhibition and binding thermodynamics between fosmidomycin and Trp203 variants, with unexpected results that may have implications for inhibitor design.

EXPERIMENTAL PROCEDURES

Materials. All chemicals were of analytical or reagent grade and were used without further purification unless otherwise stated. Glucose-6-phosphate dehydrogenase (G6PDH, yeast) was purchased from Calzyme. Glycerol-3-phosphate dehydrogenase was purchased from Roche. Fructose-1,6-diphosphate (FDP) aldolase (rabbit muscle) was purchased from Sigma. *M. tuberculosis* DXR¹⁷ and *Escherichia coli* DXP synthase¹⁸ were expressed and purified as reported previously, and their concentrations were determined spectrophotometrically using the respective extinction coefficients ($\epsilon_{280} = 37500 \text{ M}^{-1} \text{ cm}^{-1}$ for MtDXR, and $\epsilon_{280} = 50310 \text{ M}^{-1} \text{ cm}^{-1}$ for DXS) calculated from their amino acid sequence using the ProtParam utility¹⁹ and verified by the Bradford assay. Dibenzyl 3-[(benzyloxyamino)propyl]phosphonate was prepared as described by Ortmann et al.²⁰ with the following modifications. (1) The reductive amination of dibenzyl (3-oxopropyl)phosphonate with O-benzylhydroxylamine hydrochloride and sodium cyanoborohydride was maintained at pH 3 by dropwise addition of concentrated HCl in the presence of an indicator, and (2) following the published workup, the product was purified by flash chromatography with 100% ethyl acetate. Fosmidomycin was prepared from dibenzyl 3-[(benzyloxyamino)propyl]phosphonate by N-formylation and hydrogenolysis, as described by Haemers et al.²¹

Site-Directed Mutagenesis. Mutants were prepared according to the protocol of the QuikChange Site-Directed Mutagenesis Kit (Agilent). Oligonucleotide pairs that were used to introduce mutations in the forward and reverse directions are listed below, with the mutated nucleotides underlined: W203G, 5'-GGTGCCACCCGACTGGGTCCTGG-3' (forward) and 5'-CCATGGACCCAGTCGGGTGG-GCACC-3' (reverse); W203A, 5'-TGCCCACCCGACTGCG-TCCATGGGTCCG-3' (forward) and 5'-CGGACCCATGG-ACGCAGTCGGGTGGGCACC-3' (reverse); W203F, 5'-

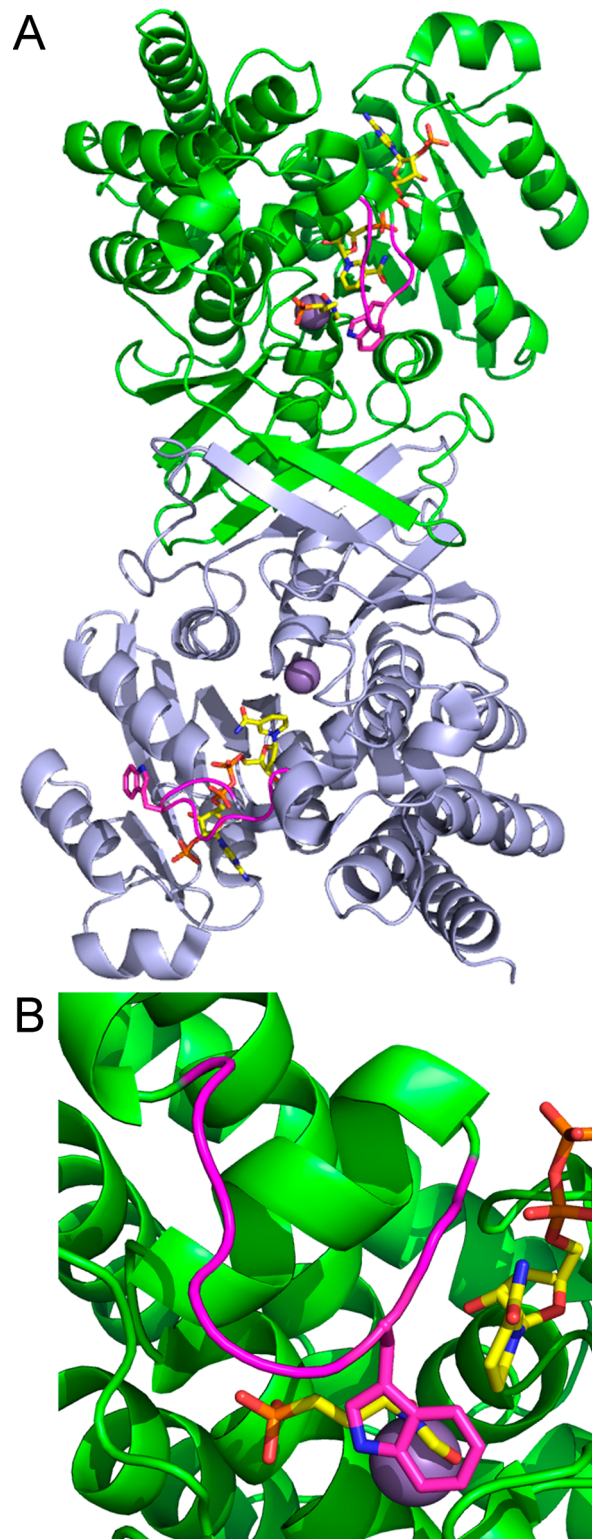


Figure 1. Structure of MtDXR in complex with fosmidomycin, NADPH, and Mn²⁺. (A) The structure (PDB entry 4AIC) of the MtDXR dimer (green and gray subunits) shows that the flexible loop (magenta) containing Trp203 exists in closed and open conformations when the active site is bound and not bound to fosmidomycin, respectively. (B) Close-up of the active site of the subunit bound with fosmidomycin.

GGTGCCACCCGACTTTCTCCATGG-3' (forward) and 5'-CGGACCCATGGGAAAGTCGGGTGGGCACC-3' (re-

verse); W203Y, 5'-GGTGCCCCACCCGACTTATTCCATGG-3' (forward) and 5'-CGGACCCATGGAATAAGTCGGGTG-GGCACC-3' (reverse). All mutations were confirmed by automated DNA sequencing.

Synthesis of 1-Deoxy-D-xylulose 5-Phosphate (DXP). The dicalcium salt of fructose 1,6-diphosphate (FDP) was used as starting material, as it was more economical than the alternatives. To a 20 mL stirred aqueous suspension containing 4.0 g of the dicalcium salt was added Amberlite IR-120(H⁺) portionwise until the suspension cleared.²² The supernatant was adjusted to pH 7 with solid K₂CO₃, resulting in the formation of a white precipitate. Following centrifugation at 15000g for 4 min, the supernatant was assayed for FDP using FDP aldolase and glycerol-3-phosphate dehydrogenase, and this served as the starting material for DXP synthesis, as previously described.²³ The progress of the reaction was monitored by a spectrophotometric assay with MtDXR. DXP was converted to the barium salt by the addition of 1 molar equiv of Ba(OH)₂·8H₂O, added portionwise with stirring and pH adjustment with glacial AcOH to maintain a pH of 7.0–7.5. After centrifugation at 15000g for 10 min at 4 °C, the supernatant was concentrated to ~20 mL by rotary evaporation, resulting in additional precipitate. After a second round of centrifugation, the supernatant was diluted with 3 volumes of EtOH and incubated in a dry ice/EtOH bath for 30–40 min. The resulting suspension was centrifuged at 15000g for 10 min at 4 °C, the supernatant was removed, and the remaining barium salt was desiccated to a constant weight. To a stirred suspension of the barium salt (1.3 g) in 55 mL of H₂O was added 0.5 M HCl dropwise until a clear solution was obtained (pH ~5.5). Na₂SO₄ (0.5 M) was added dropwise until no additional BaSO₄ precipitate was formed. After centrifugation at 15000g for 10 min, the supernatant was decolorized with activated charcoal [1% (w/v), previously rinsed of impurities with EtOH]. After the charcoal had been pelleted, the supernatant was passed through a 0.45 μm syringe filter, and the resulting solution of DXP, sodium salt was purified on cellulose, as previously described.^{5,17}

Steady-State Kinetics and Inhibition by Fosmidomycin. The NADPH stock concentration and initial velocities were determined spectrophotometrically at 340 nm ($\epsilon_{340} = 6.22 \text{ mM}^{-1} \text{ cm}^{-1}$).²⁴ DXP and fosmidomycin stock concentrations were determined by ¹H nuclear magnetic resonance (NMR) (120 s delay between transients) with 5 mM imidazole as an internal standard.^{17,25} In the absence of inhibitor, reactions were initiated at 25 °C by the addition of 10–66 nM MtDXR to cuvettes (final volume of 1.0 mL) containing DXP (31–5800 μM), 200 μM NADPH, 50 mM Tris-HCl (pH 7.5), and 10 mM MgCl₂. Data were fit with eq 1 by nonlinear regression using Kaleidagraph (Synergy Corp.) to determine apparent k_{cat} (left form), k_{cat}/K_m (right form), and K_m

$$v_0 = \frac{k_{\text{cat}}[E]_t[\text{DXP}]}{K_m + [\text{DXP}]} = \frac{(k_{\text{cat}}/K_m)[E]_t[\text{DXP}]}{1 + [\text{DXP}]/K_m} \quad (1)$$

where [E]_t is the total enzyme concentration. For inhibition assays, reactions were initiated at 25 °C by the addition of 10 nM MtDXR to cuvettes (final volume of 1.0 mL) containing fosmidomycin (0–10 μM), 1 or 2 mM DXP, 200 μM NADPH, 50 mM Tris-HCl (pH 7.5), and 10 mM MgCl₂. Because of the slow onset of inhibition by fosmidomycin, reaction velocities were measured after a steady state had been attained (~1–5 min).

Pre-Steady-State Kinetics. Pre-steady-state kinetics were measured with an Applied Photophysics SX-20 stopped-flow spectrophotometer fit with a 20 μL flow cell (10 mm path length) with a dead time of 1.08 ms. Transients from four to six repeat drives were averaged for all stopped-flow assays. The reaction chamber and all reagents were thermostated at 25.0 °C with a circulating water bath. Both syringes contained 50 mM Tris-HCl (pH 7.5), 10 mM MgCl₂, and 200 μM NADPH. One syringe additionally contained DXP (final concentrations after mixing of 5.0, 7.0, and 10 mM for wild-type MtDXR, W203F, and W203Y, respectively), and the other syringe additionally contained MtDXR (final concentrations after mixing of 10, 10, and 20 μM for wild-type MtDXR, W203F, and W203Y, respectively). The NADPH absorbance decay at 340 nm ($\epsilon_{340} = 6.22 \text{ mM}^{-1} \text{ cm}^{-1}$) was monitored for 2 s. The regions of the transients including the burst and linear steady-state region were fit with eq 2 by nonlinear regression using Pro-DataViewer (Applied Photophysics)

$$A_t = (\Delta A)e^{-k_{\text{burst}}t} + v_{ss}t + c \quad (2)$$

where ΔA is the amplitude of the burst, k_{burst} is the apparent first-order rate constant, and v_{ss} is the steady-state rate, governed by the Michaelis–Menten equation (eq 1), following the burst.

Synthesis of (4S)-[4-²H]₁NADPH (NADPD). NADPD was synthesized on a 0.3 mmol scale as previously described^{26,27} with some modifications. The oxidized form of nicotinamide adenine dinucleotide phosphate (NADP) (260 mg, 0.316 mmol) was incubated with 130 mg (0.721 mmol) of D-[1-²H]glucose (98 atom % D) in 83 mM potassium phosphate (pH 8.0) containing 40% (v/v) dimethyl sulfoxide in a final volume of 23 mL. The reaction was initiated with 2.5 mg (50 units, as determined by the manufacturer) of G6PDH and the mixture incubated at 30 °C. The progress of the reaction was assessed by monitoring the A_{260}/A_{340} ratio. After 100 min, the A_{260}/A_{340} ratio reached a plateau of ~3.6, indicating completion of the reaction. Ice-cold ethanol (270 mL, 12 volumes) was added, and the sample was incubated at –20 °C for 1 h. A white precipitate was recovered by centrifugation for 15 min at 15000g and 4 °C. After being briefly air-dried, the pellet was resuspended in 2.0 mL of 1 mM Tris-HCl (pH 8.0) and 200 mM NaCl. The crude NADPD product was purified by reversed-phase high-performance liquid chromatography (HPLC) with a semipreparative C18 column (Vydac, 5 μm, 22 mm × 250 mm). The C18 column was pre-equilibrated with 1 mM Tris-HCl (pH 8.0) and 200 mM NaCl at a flow rate of 8 mL min⁻¹. After the first 8–10 min, NADPD began to elute as indicated by A_{340} . At this point, solvent was switched to 100% methanol, and all fractions with absorbance at 340 nm were collected and pooled. To promote the stability of NADPD,²⁸ the pH of the pooled fractions was quickly increased via the addition of 1 M Tris-HCl (pH 9.2) to a final concentration of 10 mM, and the resultant solution was stored overnight at 4 °C without decomposition. After rotary evaporation to dryness, the material was redissolved in 25 mL of 10 mM triethylammonium bicarbonate (TEAB) (pH 7.7) and subsequently desalted in 5 mL portions by reversed-phase HPLC using a C18 column (Teledyne/ISCO RediSep RF high-performance Gold). The column was pre-equilibrated in 10 mM TEAB buffer, and samples were applied by syringe at a flow rate not exceeding 30 mL min⁻¹. After the sample had been washed with an additional 20 mL of TEAB buffer, NADPD was eluted with 20 mL of 100% methanol. Fractions (1.5 mL) were collected

and assayed for chloride content by being mixed with an aqueous AgNO_3 solution. Fractions (elution volume of 16.5–31.5 mL) containing NADPD (by A_{340}) and no chloride were pooled and concentrated by rotary evaporation to remove methanol (confirmed by ^1H NMR). The final NADPD solution, displaying an A_{260}/A_{340} ratio of ~3, was frozen and stored at -20°C .

Primary Deuterium Kinetic Isotope Effects. Kinetic isotope effects on k_{cat} and k_{cat}/K_m were determined simultaneously by global data fitting to eq 3 using SigmaPlot (Systat)

$$v_0 = \frac{V[\text{DXP}]}{K_m(1 + FE_{V/K}) + [\text{DXP}](1 + FE_V)} \quad (3)$$

where V is the maximal velocity, F_i is the fraction of deuterium in NADPH (0 or 1), and $E_{V/K}$ and E_V are the kinetic isotope effects minus 1 on k_{cat}/K_m (V/K) and k_{cat} (V), respectively.

Isothermal Titration Calorimetry. A VP-ITC calorimeter (GE, formerly MicroCal) equilibrated to 298 K was used for all measurements. Pilot studies revealed that over the time course of injections (2–3 h), a small amount of *MtDXR* aggregation had occurred, leading to a ligand-independent release of heat at later injections (data not shown). This behavior was avoided by dialysis of the concentrated protein for 2 h at 298 K against 50 mM Tris-HCl (pH 7.5), 10 mM MgCl_2 , and 5% glycerol, followed by centrifugation for 10 min at 13000 rpm to remove insoluble material. For each ITC experiment, the calorimeter cell was loaded with 10–15 μM *MtDXR* (monomers), 200 μM NADPH, 50 mM Tris-HCl (pH 7.5), 10 mM MgCl_2 , and 1.7% glycerol. The injection syringe was loaded with the identical solution except with 50 μM fosmidomycin in place of the enzyme. After an initial injection of 5 μL , each injection was 10 μL . Values of ΔH° , ΔS° , K_{assoc} and stoichiometry (n) were determined by fitting with MicroCal software. Because n was always close to but less than 1 when all four parameters were allowed to vary, it was assumed that the active monomer concentration was lower than that determined by A_{280} ; thus, following the recommended practice,^{29,30} the monomer concentration input into the software was decreased until n was calculated to be 1.00, at which point it was fixed and the other three parameters were determined again. Values of ΔG° and K_d were calculated using the thermodynamic relationships $\Delta G^\circ = -RT \ln K_{\text{assoc}}$ and $K_d = 1/K_{\text{assoc}}$.

Determination of the Structure of DXR Trp203 Mutants. The Trp203 mutant proteins were used for crystallization experiments. The protein retained the purification tag. Crystals of *MtDXR* grew under multiple conditions that were screened to identify the best crystals of each mutant protein. Crystals of W203F were grown by hanging drop vapor diffusion using a mother liquor containing 30% PEG 8000, 200 mM NH_4OAc , and 50 mM MES (pH 6.5). Crystals were harvested and cryoprotected using Paratone-N oil and cryocooled directly in liquid nitrogen. The W203F crystal was used for diffraction experiments at Stanford Synchrotron Radiation Lightsource (SSRL) beamline 7-1. The crystal indexed to a tetragonal space group as seen previously with *M. tuberculosis* DXR bound to the antibiotic FR-900098 (PDB entry 4A03).¹⁶ Crystals of W203Y grew via hanging drop vapor diffusion using a mother liquor containing 6% PEG 4000, 20% MPD, and 50 mM MES (pH 5.5). The W203Y mutant crystal was mounted in a nylon loop and cryocooled in liquid nitrogen without further cryoprotection. Diffraction was performed at

SSRL beamline 9-2 and revealed a new orthorhombic space group.

The structure of W203F was determined by molecular replacement using the protein coordinates from a low-resolution structure of *MtDXR* bound to 1-deoxy-L-erythrose,¹⁵ Mn^{2+} , and NADPH that we had determined by molecular replacement from the coordinates of PDB entry 4A03. The structure of W203F was determined using the PHASER³¹ module of PHENIX to identify two protein chains in the asymmetric unit; electron density for the N-terminal purification tag and residues 1–10, as well as the final C-terminal residue, was missing, so that the final model contains residues 11–388 for both chains. The structure of W203Y was determined by molecular replacement using the protein coordinates from the W203F structure and four chains identified in the asymmetric unit. The final model of W203Y contained residues 12–387 for chain A, 12–389 for chains B and D, and 12–388 for chain C. Structures of both mutants were refined through manual model building with COOT³² and refinement with PHENIX.³³ Diffraction and refinement statistics are presented in Table 1.

RESULTS AND DISCUSSION

Steady-State Kinetics. Steady-state kinetics was determined for four Trp203 mutants of *MtDXR* (Table 2). While alteration to Gly and Ala abolished activity, the k_{cat} and k_{cat}/K_m values of the Phe and Tyr mutants remained within factors of 3

Table 1. Crystallographic Data for *MtDXR* Trp203 Mutant Complexes

	W203Y	W203F
Data Collection		
PDB entry	4OOE	4OOF
wavelength (Å)	1.284	1.127
resolution (Å)	38–1.83	30–2.3
space group	$P2_12_12_1$	$P4_32_12$
unit cell parameters (Å)		
a	112.3	107.9
b	114.2	107.9
c	133.2	136.4
R_{merge}^a	0.061 (0.247)	0.092 (0.488)
completeness (%) ^a	96.1 (86.1)	99.9 (100)
I/σ^a	16.0 (3.8)	9.9 (1.7)
no. of reflections	145456	36447
Refinement		
R factor ^a (%)	17.0	16.0
R_{free}^a (%)	21.1	21.2
Wilson B value (Å ²)	18.5	32.7
average B factor (Å ²)		
overall	17.8	33.1
solvent	29.8	36.0
fosmidomycin	14.2	28.2
root-mean-square deviation from ideal		
bond lengths (Å)	0.07	0.007
bond angles (deg)	1.15	1.14
Ramachandran (%)		
favored	98	98
outliers	0.2	0.27
Molprobity Clash Score	5.4	7.3

^aThe values in parentheses represent the statistics within the highest-resolution shell.

Table 2. Steady-State Kinetic Parameters and Primary Deuterium Kinetic Isotope Effects for Trp203 Variants^a

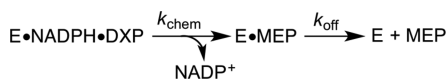
MtDXR	k_{cat} (s ⁻¹)	K_m (μM)	k_{cat}/K_m (mM ⁻¹ s ⁻¹)	${}^D V$	${}^D(V/K_{\text{DXP}})$
wild-type	4.2 ± 0.2	137 ± 12	31 ± 2	1.35 ± 0.04	2.2 ± 0.2
	5.25 ± 0.19 ^b	115 ± 7 ^b	46 ± 3 ^b	1.3 ± 0.1 ^c	2.2 ± 0.1 ^c
W203G	ND ^d	ND ^d	ND ^d	ND ^d	ND ^d
W203A	ND ^d	ND ^d	ND ^d	ND ^d	ND ^d
W203F	1.59 ± 0.10	1090 ± 120	1.46 ± 0.14	2.1 ± 0.4	2.4 ± 0.9
W203Y	3.54 ± 0.19	390 ± 20	9.1 ± 0.6	1.9 ± 0.2	2.1 ± 0.5

^aErrors (except literature values) are standard deviations from triplicate measurements. ^bDetermined by Liu and Murkin.¹⁷ ^cDetermined by Argyrou and Blanchard.¹⁸ ^dNo detectable activity.

and 20 of those of the wild type, respectively. These findings are in agreement with those of Fernandes et al.,³⁴ who mutated the corresponding Trp residue in the *Synechocystis* enzyme to Phe, Leu, Val, and Ala in an attempt to broaden the substrate specificity; all but the Phe variant were found to be particularly impaired. These data strongly suggest that DXR requires an aromatic residue in the flexible loop for effective catalysis.

Pre-Steady-State Kinetics. By monitoring transient kinetics under multiple-turnover conditions, one can often obtain kinetic information not available during steady-state measurements. In previous stopped-flow studies, when MtDXR was premixed with NADPH and then rapidly mixed with DXP, a burst in the oxidation of NADPH was observed during the first turnover.¹⁷ This burst was attributed to the slow release of MEP (k_{off}) following k_{chem} , the net rate constant that includes isomerization, reduction, and release of NADP⁺ (Scheme 2).

Scheme 2. Burst Kinetics Model for Pre-Steady-State Experiments with MtDXR



When this was repeated with W203F, the data appeared to be linear throughout the experiment (Figure 2). With W203Y, a significantly diminished burst was observed. In this case, fitting of eq 2 revealed that the burst rate (k_{burst}) relative to wild-type MtDXR had decreased from 49.7 ± 0.5 to 11 ± 2 s⁻¹, and the burst amplitude (expressed as the mole percentage of protein monomers) had decreased from 48% to 9.5%. The loss of burst

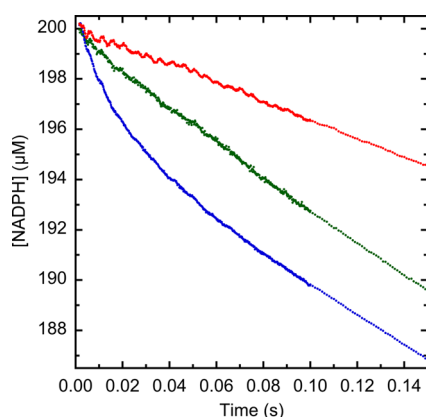


Figure 2. Pre-steady-state kinetics. The oxidation of NADPH was monitored by the decrease in absorbance at 340 nm upon mixing 5, 7, and 10 mM DXP with wild-type MtDXR (blue, 10 μM), W203F (red, 10 μM), and W203Y (green, 20 μM), respectively, in the presence of 200 μM NADPH and 10 mM MgCl₂.

behavior in the two mutants is indicative of a change in the rate-limiting step in which k_{chem} has become smaller than k_{off} . According to Scheme 2, k_{burst} is related to k_{chem} and k_{off} by eq 4 and the burst amplitude is given by eq 5.³⁵

$$k_{\text{burst}} = k_{\text{chem}} + k_{\text{off}} \quad (4)$$

$$[\text{NADP}^+]_{\text{burst}} = [\text{DXR}] \left(\frac{k_{\text{chem}}}{k_{\text{chem}} + k_{\text{off}}} \right)^2 = [\text{DXR}] \left(\frac{k_{\text{chem}}}{k_{\text{burst}}} \right)^2 \quad (5)$$

Using these equations, k_{chem} and k_{off} were calculated to be 3.3 ± 0.7 and 7.4 ± 1.3 s⁻¹, respectively, for W203Y. In contrast, the wild-type enzyme had previously been estimated to have a k_{chem} of 48.8 ± 1.9 s⁻¹ and a k_{off} of 8.4 ± 0.5 s⁻¹.¹⁷ Thus, pre-steady-state analysis confirms that mutation of Trp203, at least to Tyr, resulted in a decrease in the rate of chemistry by 1 order of magnitude while leaving the rate of MEP release essentially unchanged.

Kinetic Isotope Effects. Kinetic isotope effect (KIE) studies were pursued to confirm the change in the rate-limiting step upon mutation suggested by the pre-steady-state kinetics. KIEs are a powerful tool for establishing kinetic mechanisms, as their magnitudes not only reflect the isotope-sensitive step giving rise to the intrinsic KIE but also are sensitive to other kinetically significant steps. In enzyme-catalyzed reactions, primary deuterium KIEs can be measured on k_{cat}/K_m , symbolized ${}^D(V/K)$, or k_{cat} , symbolized ${}^D V$. These observed KIEs are related to the intrinsic KIE, ${}^D k$, moderated by forward (c_f for k_{cat}/K_m and c_{vf} for k_{cat}) and reverse (c_r) commitment factors and the equilibrium isotope effect (${}^D K_{\text{eq}}$) according to eqs 6 and 7.

$${}^D(V/K) = \frac{{}^D k + c_f + c_r {}^D K_{\text{eq}}}{1 + c_f + c_r} \quad (6)$$

$${}^D V = \frac{{}^D k + c_{vf} + c_r {}^D K_{\text{eq}}}{1 + c_{vf} + c_r} \quad (7)$$

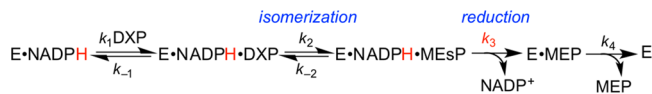
Inspection of these equations reveals that the difference between ${}^D(V/K)$ and ${}^D V$ lies solely in the respective forward commitments. As the isotope-sensitive step becomes more rate-limiting, these commitments decrease and the observed KIE increases toward the intrinsic value. On the one hand, if ${}^D(V/K)$ and ${}^D V$ are similar in magnitude, then c_f and c_{vf} are similar, and we can conclude that the isotope-sensitive step is equally rate-limiting on both steady-state parameters. On the other hand, if one of these KIEs is lower than the other, this indicates the existence of a slow step unique to that kinetic parameter.

By measuring steady-state kinetics with a varying DXP concentration and a fixed saturating NADPH or (4S)-[4-²H]NADPH (NADPD) concentration, a ${}^D(V/K)$ of $2.2 \pm$

0.2 and a ${}^D V$ of 1.35 ± 0.04 were measured for wild-type MtDXR (Table 2), in agreement with values reported by Argyrou and Blanchard using a similar MtDXR construct.¹⁸ Thus, c_{vf} is significantly greater than c_f . When Trp203 was mutated to Phe or Tyr, the ${}^D(V/K)$ values remained unchanged at 2.4 ± 0.9 and 2.1 ± 0.5 , respectively, but the ${}^D V$ values increased to 2.1 ± 0.4 and 1.9 ± 0.2 , respectively. This indicates c_{vf} was lowered by mutation to become approximately equal to c_f .

To gain insight into the significance of these forward commitment factors, it is useful to examine a kinetic mechanism operative under the conditions of the KIE measurements. Strictly, MtDXR employs a steady-state random mechanism,^{17,18} but under initial velocity conditions and with the knowledge that NADPH is a “sticky substrate” (i.e., it tends to react rather than dissociate from the ternary complex),¹⁸ a simplified steady-state ordered mechanism can be assumed, as in Scheme 3 (see the Supporting Information for a more

Scheme 3. Simplified Kinetic Model for the Kinetic Isotope Effect on the Transfer of Hydride from NADPH^a



^aThe isotope (H or D) and isotope-sensitive step are in red.

detailed account of this mechanism). c_f is given by eq 8 (note that DXP dissociation, k_{-1} , is much faster than isomerization, k_1),¹⁷ and c_{vf} is given by eq 9.

$$c_f = \frac{k_3}{k_{-2}} \left(1 + \frac{k_2}{k_{-1}} \right) \approx \frac{k_3}{k_{-2}} \quad (8)$$

$$c_{vf} = \left(\frac{k_2 k_3}{k_2 + k_{-2}} \right) \left(\frac{1}{k_2} + \frac{1}{k_4} \right) \quad (9)$$

For wild-type MtDXR, c_{vf} is larger than c_f because of the slow release of MEP, k_4 (equivalent to k_{off} in Scheme 2), which is consistent with the burst behavior observed in pre-steady-state kinetics. For the two mutants, the nearly equivalent c_f and c_{vf} values indicate that MEP dissociation is no longer significant (i.e., $k_2 < k_4$), consistent with the loss of burst kinetics, and c_{vf} can be approximated by eq 10.

$$c_{vf} = \frac{k_3}{k_2 + k_{-2}} \quad (10)$$

Further, the fact that c_{vf} is nearly equal to c_f implies that isomerization from DXP to MEsP is not favored (i.e., $k_2 < k_{-2}$). Therefore, regardless of the DXP concentration, only the

isomerization (k_2 and k_{-2}) and reduction (k_3) steps contribute to the rate upon mutation of Trp203. This finding establishes a functional link between the flexible loop and chemical barrier crossing.

Inhibition by Fosmidomycin. Despite extensive medicinal chemistry efforts, few compounds have been identified with activity rivaling fosmidomycin. Accordingly, it often serves as a reference compound for benchmarking DXR inhibition. While fosmidomycin inhibited wild-type MtDXR with a K_i of 93 ± 10 nM, it surprisingly exhibited more potent inhibition of W203F (60 ± 20 nM) and W203Y (14 ± 2 nM) (Table 3). Considering that each variant has a unique K_m for DXP, the K_m/K_i ratio provides a more realistic description of the relative specificity of each for fosmidomycin over the substrate; thus, as tryptophan is changed to phenylalanine or tyrosine, the K_m/K_i increases from 1500 to 18000 or 28000, respectively (Table 3).

Thermodynamics of Fosmidomycin Binding. The reason for the enhanced preference for binding of fosmidomycin to the Trp203 mutants was not immediately apparent; therefore, isothermal titration calorimetry (ITC) was performed in an attempt to dissect the binding energy into enthalpic and entropic components. Previous ITC studies with MtDXR have been reported at 279 K because its protein stability is better at lower temperatures.⁹ Consistent with this observation, the preparations of Trp203 mutants displayed some precipitation over prolonged incubations at 298 K, which was used in our kinetic and inhibition studies. Because we desired to maintain this temperature for all experiments, 1.7% glycerol was included in the calorimeter cell and syringe, which successfully stabilized the proteins throughout the titrations without interfering with the binding thermodynamics. Fosmidomycin was titrated against each enzyme in the presence of 200 μ M NADPH and 10 mM MgCl₂ at pH 7.5 and 298 K (Figure 3). The dissociation constant in each case was ~2-fold lower than the respective inhibition constant but followed the same order: wild type > W203F > W203Y (Table 3). The K_d of 59 ± 5 nM for wild-type MtDXR is lower than the value of 290 nM reported at 279 K with 2 mM MnCl₂.⁹ The reason for the discrepancy is not apparent, as lower temperatures are expected to yield tighter affinity for exothermic binding, and the nature of the metal (i.e., Mg²⁺ vs Mn²⁺) was shown not to be significant for binding of fosmidomycin to *E. coli* DXR.⁹ The free energy of binding to wild-type MtDXR was found to be evenly distributed between enthalpy and entropy (Table 3). Strikingly, when Trp203 was mutated, the binding enthalpy became more exothermic by 2.8 kcal/mol (W203F) and 5.4 kcal/mol (W203Y), exceeding the reduction in entropy of 2.5 kcal/mol (W203F) and 4.0 kcal/mol (W203Y), respectively. Thus, mutation of this residue to

Table 3. Inhibition and Binding Thermodynamics for Fosmidomycin^a

MtDXR	K_i (nM) ^b	K_m/K_i	K_d (nM) ^c	ΔG° (kcal/mol)	ΔH° (kcal/mol)	$-T\Delta S^\circ$ (kcal/mol)
wild-type	93 ± 10	1500	59 ± 5	-9.82 ± 0.08	-4.8 ± 0.7	-5.0 ± 0.7
	140^{d}		290^e	-8.34^e	-6.0^e	-2.3^e
W203F	60 ± 20	18000	37 ± 2	-10.10 ± 0.05	-7.6 ± 0.7	-2.5 ± 0.7
W203Y	14 ± 2	28000	5.2 ± 1.0	-11.26 ± 0.19	-10.2 ± 0.3	-1.0 ± 0.4

^aMeasured at 298 K and pH 7.5 in the presence of 10 mM MgCl₂. Errors are standard deviations from duplicate or triplicate measurements.

^bMeasured by the competitive inhibition assay. ^cCalculated as the reciprocal of the association constant determined by isothermal titration calorimetry. ^dDetermined by Deng et al.⁴¹ using 4 mM MgCl₂ at 303 K and pH 7.6 and using a DXP K_m of 47.1 μ M from Dhiman et al.⁴²

^eDetermined by Cai et al.⁹ using 2 mM MnCl₂ at 276 K and pH 7.6.

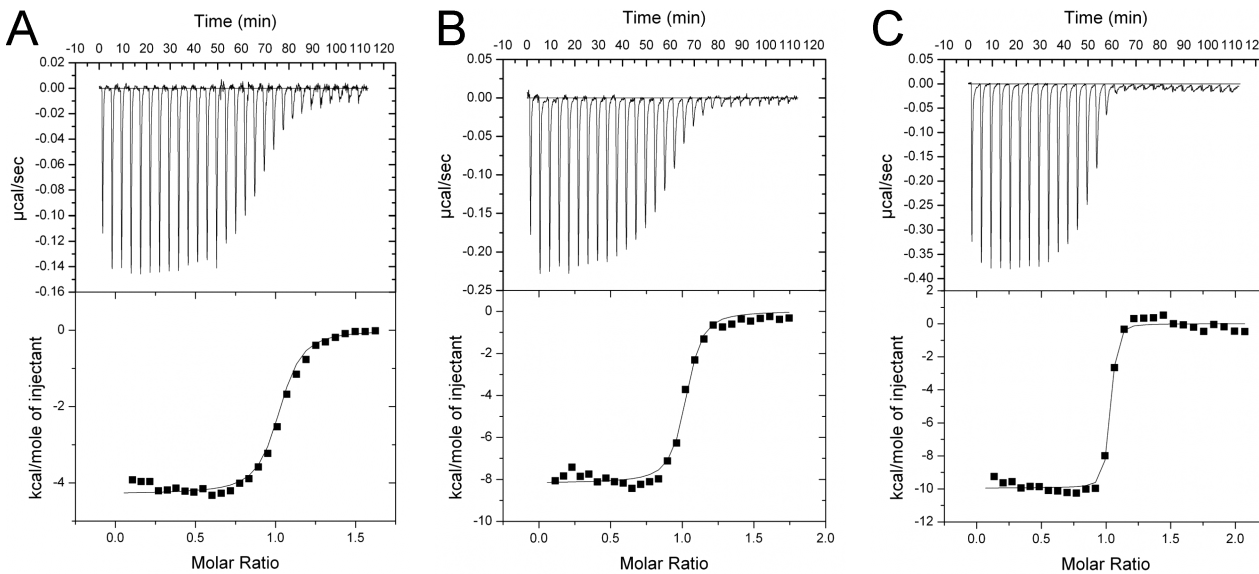


Figure 3. Isothermal titration calorimetry of fosmidomycin binding to (A) wild-type MtDXR, (B) W203F, and (C) W203Y.

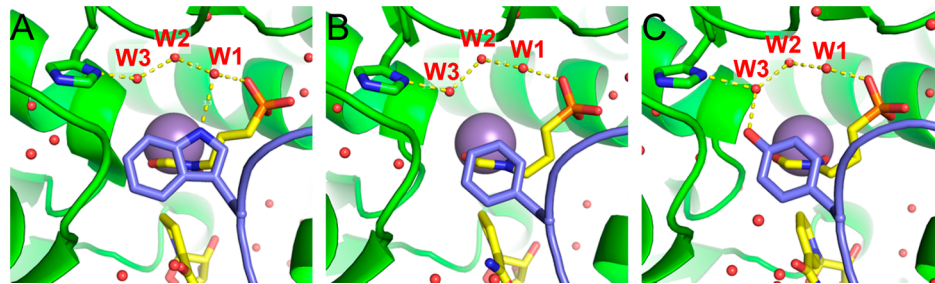


Figure 4. Active-site structures of (A) wild-type MtDXR (PDB entry 4AIC), (B) W203F, and (C) W203Y in complex with fosmidomycin, NADPH, and Mn²⁺. Possible hydrogen bonds (yellow dashed lines) are shown connecting His248, three water molecules (W1–W3), the inhibitor's phosphonate group, and Trp203 or Tyr203.

Phe and Tyr resulted in 75% and 91% enthalpy-driven binding of fosmidomycin, respectively.

The origin of the elevated binding enthalpy when altering Trp203 is not immediately clear. The major exothermic contributions to binding are noncovalent interactions formed in the enzyme–inhibitor complex, while the major endothermic contributions are hydrogen bonds in the unliganded enzyme between the protein and bound water molecules, which must be displaced to accommodate the inhibitor. When binding becomes more exothermic, as in the case of the Trp203 mutants, one of three situations is most likely involved: (1) the bound complex experiencing a net increase in the strength of noncovalent interactions, (2) the unliganded protein being less hydrated, or (3) a combination of both. On one hand, when considering only noncovalent interactions, the hydrophobicity of residue 203 cannot be the major determinant because changes to more hydrophobic (i.e., Phe) and less hydrophobic (i.e., Tyr) side chains both resulted in more exothermic binding. Alternatively, the binding enthalpy may be influenced by differences in hydrogen bonding to this residue in the enzyme–inhibitor complex (*vide infra*). On the other hand, when considering the unliganded enzymes and in the absence of large changes in protein conformation that would be unexpected for this point mutation, W203Y would be assumed to be the most hydrated because of phenol's polarity and potential for forming hydrogen bonds; this would have resulted in less exothermic binding, which was not observed.

Structural Investigation of MtDXR Trp203 Variants.

To address the surprising differences in the enthalpy of binding of fosmidomycin to the Trp203 variants, the crystal structures of W203F and W203Y in the presence of Mn²⁺, fosmidomycin, and NADPH were determined using diffraction data to 2.3 and 1.8 Å, respectively. The active sites of all protein chains in W203F and W203Y showed electron density for all three ligands. This result differs from the published structure of wild-type MtDXR (PDB entry 4AIC), which showed only one of the two subunits was occupied by fosmidomycin (Figure 1A), but is similar to the structure bound with the analogous inhibitor FR-900098 (the acetyl derivative of fosmidomycin), which features fully occupied active sites (PDB entry 4A03).¹⁶ Comparison of the structural deviation between any pairs of chains between the mutant and closed wild-type structures gave a root-mean-square displacement of <0.4 Å between all C_α atoms, demonstrating that there are no large conformational changes to the structures. The aromatic side chains of the wild-type and mutant enzymes all adopt the same torsional angles and fill a hydrophobic pocket formed by Pro265 and Met267. The additional residues within 4 Å of the Trp203 side chain of wild-type MtDXR, Ser245 and His248, are unchanged in the mutants.

In the three fosmidomycin-bound MtDXR structures, the inhibitor's phosphonate moiety not only makes contacts with active-site residues (Ser213, Asn218, Ser177, and Lys219) but also forms a hydrogen bond with one of three water molecules

that form a hydrogen bond network to His248 (Figure 4), a residue that is critical for DXP binding and turnover.³⁶ Although the positions of these water molecules are essentially unchanged among the variants, residue 203 appears to impinge upon this water network. In particular, the indole nitrogen of Trp203 is 3.3 Å from the water molecule (W1) that interacts directly with the phosphonate group, and therefore, Trp203 may serve as a hydrogen bond donor. Whereas W203F lacks the ability to hydrogen bond, the phenolic oxygen of Tyr203 in W203Y makes a 2.6 Å hydrogen bond to the third water molecule (W3) in the network. On the basis of the observed enthalpy differences, one may speculate that residue 203 attenuates the strength of the water network. Accordingly, using W203F as a reference point, the Trp–W1 hydrogen bond in wild-type *MtDXR* disrupts the water network and therefore moderately destabilizes the complex. In contrast, the Tyr–W3 hydrogen bond may reinforce the water network, significantly stabilizing its complex.

It is important to note that we cannot exclude differences in hydration of the unliganded complexes as a contributor to the increased binding enthalpy exhibited by W203F and W203Y relative to that of wild-type *MtDXR* (*vide supra*). Greater hydration of the unliganded wild-type enzyme could result from the surface area of the indole group being larger than those of benzene and phenol, requiring more ordered water molecules in its vicinity. Alternatively, this could be the result of structural differences among the variants in their unbound states. Attempts to crystallize the proteins in the absence of fosmidomycin were unsuccessful, so a structural basis for evaluating this possibility cannot be found. Nevertheless, in light of the low root-mean-square displacements observed for the backbones of the enzyme–inhibitor complexes, we expect the unbound complexes to be similarly superimposable and thus similarly hydrated.

CONCLUSIONS AND IMPLICATIONS FOR INHIBITOR DESIGN

On the basis of structural data, several groups have considered DXR's conserved flexible loop an essential catalytic element.^{14,15,37–39} By demonstrating a change in the rate-limiting step upon alteration of Trp203 in this loop, we have established a functional link between this structural element and chemical barrier crossing. The inhibition and binding studies with fosmidomycin reinforce the importance of the loop as a determinant in ligand association. Most importantly, the results of the calorimetry study suggest a significant amount of untapped binding energy might be exploited through formation of new interactions between an inhibitor and the loop, either directly or via the active-site water network. Thus, rather than realizing this binding potential through alteration of the protein, as described in this work, we envision construction of fosmidomycin derivatives with polar moieties extending from its propyl backbone. Although DXR's active site is intolerant to many substitutions to the fosmidomycin core, substituents at the position α to the phosphonate have been well accommodated.^{21,40}

ASSOCIATED CONTENT

Supporting Information

Derivation of the steady-state mechanism shown in Scheme 3 and Michaelis–Menten and Lineweaver–Burk plots for deuterium KIEs. This material is available free of charge via the Internet at <http://pubs.acs.org>.

AUTHOR INFORMATION

Corresponding Author

*E-mail: amurkin@buffalo.edu. Telephone: (716) 645-4249. Fax: (716) 645-6963.

Author Contributions

S.A.K. and G.T. contributed equally to this work.

Funding

This work was supported by a DuPont Young Professor Grant and NSF CAREER Award CHE1255136 (to A.S.M.) and National Institutes of Health Grant GM-068440 (to A.M.G.).

Notes

The authors declare no competing financial interest.

ABBREVIATIONS

DXP, 1-deoxy-D-xylulose 5-phosphate; DXR, 1-deoxy-D-xylulose-5-phosphate reductoisomerase; ED, enediolate [(Z)-propene-1,2-diolate]; FDP, D-fructose 1,6-diphosphate; G6PDH, glucose-6-phosphate dehydrogenase; GP, glycolaldehyde 2-phosphate; ITC, isothermal titration calorimetry; MEP, 2-C-methyl-D-erythritol 4-phosphate; MEsP, 2-C-methyl-D-erythrose 4-phosphate; NADP⁺, oxidized form of nicotinamide adenine dinucleotide phosphate; NADPH, reduced form of nicotinamide adenine dinucleotide phosphate; NADPD, (4S)-[4²H]NADPH; PDB, Protein Data Bank; TEAB, triethylammonium bicarbonate.

REFERENCES

- (1) Miziorko, H. M. (2011) Enzymes of the mevalonate pathway of isoprenoid biosynthesis. *Arch. Biochem. Biophys.* 505, 131–143.
- (2) Lange, B. M., Rujan, T., Martin, W., and Croteau, R. (2000) Isoprenoid biosynthesis: The evolution of two ancient and distinct pathways across genomes. *Proc. Natl. Acad. Sci. U.S.A.* 97, 13172–13177.
- (3) Grawert, T., Groll, M., Rohdich, F., Bacher, A., and Eisenreich, W. (2011) Biochemistry of the non-mevalonate isoprenoid pathway. *Cell. Mol. Life Sci.* 68, 3797–3814.
- (4) Manning, K. A., Sathyamoorthy, B., Eletsky, A., Szyperski, T., and Murkin, A. S. (2012) Highly precise measurement of kinetic isotope effects using ¹H-detected 2D [¹³C,¹H]-HSQC NMR spectroscopy. *J. Am. Chem. Soc.* 134, 20589–20592.
- (5) Munos, J. W., Pu, X., Mansoorabadi, S. O., Kim, H. J., and Liu, H. W. (2009) A secondary kinetic isotope effect study of the 1-deoxy-D-xylulose-5-phosphate reductoisomerase-catalyzed reaction: Evidence for a retroaldol-aldol rearrangement. *J. Am. Chem. Soc.* 131, 2048–2049.
- (6) Jawaid, S., Seidle, H., Zhou, W., Abdirahman, H., Abadeer, M., Hix, J. H., van Hoek, M. L., and Couch, R. D. (2009) Kinetic characterization and phosphoregulation of the *Francisella tularensis* 1-deoxy-D-xylulose 5-phosphate reductoisomerase (MEP synthase). *PLoS One* 4, e8288.
- (7) Kuzuyama, T., Shimizu, T., Takahashi, S., and Seto, H. (1998) Fosmidomycin, a specific inhibitor of 1-deoxy-D-xylulose 5-phosphate reductoisomerase in the nonmevalonate pathway for terpenoid biosynthesis. *Tetrahedron Lett.* 39, 7913–7916.
- (8) Koppisch, A. T., Fox, D. T., Blagg, B. S., and Poulter, C. D. (2002) *E. coli* MEP synthase: Steady-state kinetic analysis and substrate binding. *Biochemistry* 41, 236–243.
- (9) Cai, G., Deng, L., Fryszczyn, B. G., Brown, N. G., Liu, Z., Jiang, H., Palzkill, T., and Song, Y. (2012) Thermodynamic Investigation of Inhibitor Binding to 1-Deoxy-D-Xylulose-5-Phosphate Reductoisomerase. *ACS Med. Chem. Lett.* 3, 496–500.
- (10) Borrmann, S., Lundgren, I., Oyakhirome, S., Impouma, B., Matsiegui, P. B., Adegnika, A. A., Issifou, S., Kun, J. F. J., Hutchinson, D., Wiesner, J., et al. (2006) Fosmidomycin plus clindamycin for

- treatment of pediatric patients aged 1 to 14 years with *Plasmodium falciparum* malaria. *Antimicrob. Agents Chemother.* 50, 2713–2718.
- (11) Jomaa, H., Wiesner, J., Sanderbrand, S., Altincicek, B., Weidemeyer, C., Hintz, M., Turbachova, I., Eberl, M., Zeidler, J., Lichtenthaler, H. K., et al. (1999) Inhibitors of the nonmevalonate pathway of isoprenoid biosynthesis as antimarial drugs. *Science* 285, 1573–1576.
- (12) Brown, A. C., and Parish, T. (2008) Dxr is essential in *Mycobacterium tuberculosis* and fosmidomycin resistance is due to a lack of uptake. *BMC Microbiol.* 8.
- (13) Uh, E., Jackson, E. R., Jose, G. S., Maddox, M., Lee, R. E., Lee, R. E., Boshoff, H. I., and Dowd, C. S. (2011) Antibacterial and antitubercular activity of fosmidomycin, FR900098, and their lipophilic analogs. *Bioorg. Med. Chem. Lett.* 21, 6973–6976.
- (14) Henriksson, L. M., Unge, T., Carlsson, J., Aqvist, J., Mowbray, S. L., and Jones, T. A. (2007) Structures of *Mycobacterium tuberculosis* 1-deoxy-D-xylulose-5-phosphate reductoisomerase provide new insights into catalysis. *J. Biol. Chem.* 282, 19905–19916.
- (15) Kholodar, S. A., and Murkin, A. S. (2013) DXP Reductoisomerase: Reaction of the Substrate in Pieces Reveals a Catalytic Role for the Nonreacting Phosphodianion Group. *Biochemistry* 52, 2302–2308.
- (16) Bjorkelid, C., Bergfors, T., Unge, T., Mowbray, S. L., and Jones, T. A. (2012) Structural studies on *Mycobacterium tuberculosis* DXR in complex with the antibiotic FR-900098. *Acta Crystallogr. D68*, 134–143.
- (17) Liu, J., and Murkin, A. S. (2012) Pre-steady-state kinetic analysis of 1-deoxy-D-xylulose-5-phosphate reductoisomerase from *Mycobacterium tuberculosis* reveals partially rate-limiting product release by parallel pathways. *Biochemistry* 51, 5307–5319.
- (18) Argyrou, A., and Blanchard, J. S. (2004) Kinetic and chemical mechanism of *Mycobacterium tuberculosis* 1-deoxy-D-xylulose-5-phosphate isomero-reductase. *Biochemistry* 43, 4375–4384.
- (19) Gasteiger, E., Hoogland, C., Gattiker, A., Duvaud, S., Wilkins, M. R., Appel, R. D., and Bairoch, A. (2005) Protein identification and analysis tools on the ExPASy server. In *The Proteomics Protocols Handbook* (Walker, J. M., Ed.) pp 571–607, Humana Press, Totowa, NJ.
- (20) Ortmann, R., Wiesner, J., Silber, K., Klebe, G., Jomaa, H., and Schlitzer, M. (2007) Novel deoxysxylulosephosphate-reductoisomerase inhibitors: Fosmidomycin derivatives with spacious acyl residues. *Arch. Pharm. (Weinheim, Ger.)* 340, 483–490.
- (21) Haemers, T., Wiesner, J., Busson, R., Jomaa, H., and Van Calenbergh, S. (2006) Synthesis of α-Aryl-Substituted and Conformationally Restricted Fosmidomycin Analogues as Promising Antimalarials. *Eur. J. Org. Chem.* 2006, 3856–3863.
- (22) Durrwachter, J. R., Drueckhammer, D. G., Nozaki, K., Sweers, H. M., and Wong, C. H. (1986) Enzymatic Aldol Condensation Isomerization as a Route to Unusual Sugar-Derivatives. *J. Am. Chem. Soc.* 108, 7812–7818.
- (23) Taylor, S. V., Vu, L. D., Begley, T. P., Schorken, U., Grolle, S., Sprenger, G. A., Bringer-Meyer, S., and Sahm, H. (1998) Chemical and enzymatic synthesis of 1-Deoxy-D-xylulose-5-phosphate. *J. Org. Chem.* 63, 2375–2377.
- (24) Dawson, R. M. C., Elliott, D. C., Elliott, W. H., and Jones, K. M. (1986) *Data for Biochemical Research*, 3rd ed., Clarendon Press, Oxford, U.K.
- (25) O'Donoghue, A. C., Amyes, T. L., and Richard, J. P. (2005) Hydron transfer catalyzed by triosephosphate isomerase. Products of isomerization of (R)-glyceraldehyde 3-phosphate in D₂O. *Biochemistry* 44, 2610–2621.
- (26) Pollock, V. V., and Barber, M. J. (2001) Kinetic and mechanistic properties of biotin sulfoxide reductase. *Biochemistry* 40, 1430–1440.
- (27) Viola, R. E., Cook, P. F., and Cleland, W. W. (1979) Stereoselective preparation of deuterated reduced nicotinamide adenine nucleotides and substrates by enzymatic synthesis. *Anal. Biochem.* 96, 334–340.
- (28) Markham, K. A., and Kohen, A. (2006) Analytical procedures for the preparation, isolation, analysis and preservation of reduced nicotinamides. *Curr. Anal. Chem.* 2, 379–388.
- (29) Ghai, R., Falconer, R. J., and Collins, B. M. (2012) Applications of isothermal titration calorimetry in pure and applied research: Survey of the literature from 2010. *J. Mol. Recognit.* 25, 32–52.
- (30) Turnbull, W. B., and Daranas, A. H. (2003) On the value of c: Can low affinity systems be studied by isothermal titration calorimetry? *J. Am. Chem. Soc.* 125, 14859–14866.
- (31) McCoy, A. J., Grosse-Kunstleve, R. W., Adams, P. D., Winn, M. D., Storoni, L. C., and Read, R. J. (2007) PHASER crystallographic software. *J. Appl. Crystallogr.* 40, 658–674.
- (32) Emsley, P., and Cowtan, K. (2004) COOT: Model-building tools for molecular graphics. *Acta Crystallogr. D60*, 2126–2132.
- (33) Adams, P. D., Afonine, P. V., Bunkoczi, G., Chen, V. B., Davis, I. W., Echols, N., Headd, J. J., Hung, L. W., Kapral, G. J., Grosse-Kunstleve, R. W., et al. (2010) PHENIX: A comprehensive Python-based system for macromolecular structure solution. *Acta Crystallogr. D66*, 213–221.
- (34) Fernandes, R. P., Phaosiri, C., and Proteau, P. J. (2005) Mutation in the flexible loop of 1-deoxy-D-xylulose 5-phosphate reductoisomerase broadens substrate utilization. *Arch. Biochem. Biophys.* 444, 159–164.
- (35) Johnson, K. A. (1992) Transient-State Kinetic Analysis of Enzyme Reaction Pathways. In *The Enzymes* (David, S. S., Ed.) pp 1–61, Academic Press, New York.
- (36) Kuzuyama, T., Takahashi, S., Takagi, M., and Seto, H. (2000) Characterization of 1-deoxy-D-xylulose 5-phosphate reductoisomerase, an enzyme involved in isopentenyl diphosphate biosynthesis, and identification of its catalytic amino acid residues. *J. Biol. Chem.* 275, 19928–19932.
- (37) Reuter, K., Sanderbrand, S., Jomaa, H., Wiesner, J., Steinbrecher, I., Beck, E., Hintz, M., Klebe, G., and Stubbs, M. T. (2002) Crystal structure of 1-deoxy-D-xylulose-5-phosphate reductoisomerase, a crucial enzyme in the non-mevalonate pathway of isoprenoid biosynthesis. *J. Biol. Chem.* 277, 5378–5384.
- (38) Steinbacher, S., Kaiser, J., Eisenreich, W., Huber, R., Bacher, A., and Rohdich, F. (2003) Structural basis of fosmidomycin action revealed by the complex with 2-C-methyl-D-erythritol 4-phosphate synthase (IspC). Implications for the catalytic mechanism and antimalaria drug development. *J. Biol. Chem.* 278, 18401–18407.
- (39) Yajima, S., Nonaka, T., Kuzuyama, T., Seto, H., and Ohsawa, K. (2002) Crystal structure of 1-deoxy-D-xylulose 5-phosphate reductoisomerase complexed with cofactors: Implications of a flexible loop movement upon substrate binding. *J. Biochem.* 131, 313–317.
- (40) Schlüter, K., Walter, R. D., Bergmann, B., and Kurz, T. (2006) Arylmethyl substituted derivatives of fosmidomycin: Synthesis and antimalarial activity. *Eur. J. Med. Chem.* 41, 1385–1397.
- (41) Deng, L., Diao, J., Chen, P., Pujari, V., Yao, Y., Cheng, G., Crick, D. C., Prasad, B. V., and Song, Y. (2011) Inhibition of 1-deoxy-D-xylulose-5-phosphate reductoisomerase by lipophilic phosphonates: SAR, QSAR, and crystallographic studies. *J. Med. Chem.* 54, 4721–4734.
- (42) Dhiman, R. K., Schaeffer, M. L., Bailey, A. M., Testa, C. A., Scherman, H., and Crick, D. C. (2005) 1-Deoxy-D-xylulose 5-phosphate reductoisomerase (IspC) from *Mycobacterium tuberculosis*: Towards understanding mycobacterial resistance to fosmidomycin. *J. Bacteriol.* 187, 8395–8402.